

Noncooled site-resolved imaging of a Mott insulator

Martin Miranda,* Ryotaro Inoue, Naoki Tambo, and Mikio Kozuma
*Department of Physics, Tokyo Institute of Technology,
 2-12-1 O-okayama, Meguro-ku, Tokyo 152-8550, Japan*
 (Dated: April 25, 2017)

We demonstrate site-resolved imaging of a strongly correlated quantum system without relying on laser-cooling techniques during fluorescence imaging. We observed the formation of Mott shells in the insulating regime and realized thermometry on the atomic cloud. This work proves the feasibility of the noncooled approach and opens the door to extending the detection technology to new atomic species.

Since the creation of site-resolved fluorescence imaging devices capable of observing a quantum gas trapped in a two-dimensional optical lattice[1], there has been tremendous progress in the study of strongly correlated quantum systems. Starting with the observation of the superfluid-to-Mott-insulator transition at single atom level[2, 3] using bosonic Rb atoms, scientists were able to observe the phase transition of interacting quantum Ising spins[4], dynamics of interacting quantum walkers[5] and magnon bound states[6], and also realize measurement of entanglement entropy[7]. Recently, the detection technology was expanded to fermionic Li[8, 9] and K[10–12], which culminated in the observation of a fermionic Mott insulator[13, 14] and long-range antiferromagnetic ordering[15]. These experiments are significant towards the understanding of d-wave superconductivity. Improving the site-resolved imaging technology and extending it to new atomic species is an important step to explore a broader variety of strongly correlated phenomena. Among the candidates for extending the technology, highly dipolar atoms such as Dy and Er are promising to study the extended Bose-Hubbard Model and its underlying exotic phases of matter[16, 17].

The most challenging task in the realization of site-resolved fluorescence imaging is fulfilling the requirement that atoms stay localized into the site while their fluorescence is collected. The conventional method to achieve this is to perform laser-cooling simultaneously with imaging. Different cooling methods were applied in the past experiments: polarization gradient cooling in the case of Rb[1], Raman cooling for Li[8, 9] and K[10], EIT cooling for K[11, 12], and narrow-line optical molasses for Yb[18]. Although these cooling techniques have proven to be effective to achieve imaging with near unity fidelity, the experimental setups are complicated and often only applicable to a particular species.

A promising alternative to laser-cooling based systems is to use a sufficient deep optical potential and short exposure time. This method was demonstrated using Yb atoms[19], where an optical lattice near resonant to a transition from the excited state was used to create a large light shift. The required deep potential was created by coupling the ground and excited states with an excitation beam. The main advantage of this experimen-

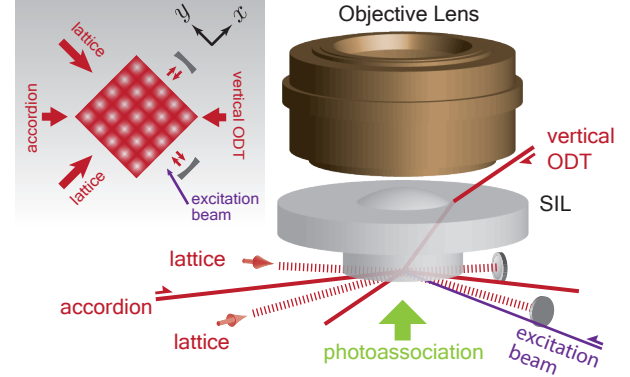


FIG. 1. Experimental setup. After creating a Bose-Einstein condensate and compressing it using a combination of an optical accordion and a vertical ODT, a pair of retro-reflected lattice beams are introduced to load the atoms into the two-dimensional optical lattice. The system is then driven into a Mott insulating state by gradually ramping up the intensity of the lattice beams. A photoassociation light is used to force inelastic light-assisted collisions on multiple occupied sites. Site-resolved imaging of the insulator is realized by irradiating a single excitation beam onto the atoms. No cooling mechanism is employed while the imaging system collects the photons.

tal setup is that it only requires a single excitation beam and an available transition from the excited state, and is thus readily extensible to new atomic species.

Up to this letter, access to strongly correlated quantum systems was limited to laser-cooling based systems, and it was not clear whether the noncooled approach would provide sufficient fidelity to access the required physics. Here, we report the first direct observation of Hubbard-system using a noncooled site-resolved imaging device. We observed the shell structure of a bosonic ^{174}Yb Mott insulator with near unity fidelity, proving the effectiveness of this approach.

The experiment starts by preparing a two-dimensional condensate of 5×10^4 bosonic ^{174}Yb positioned at $2.6 \mu\text{m}$ below the surface of a solid immersion lens (SIL). The SIL enables us to increase the resolution of the imaging system and additionally fix the position of the atoms relatively to its flat surface. The procedure to create and

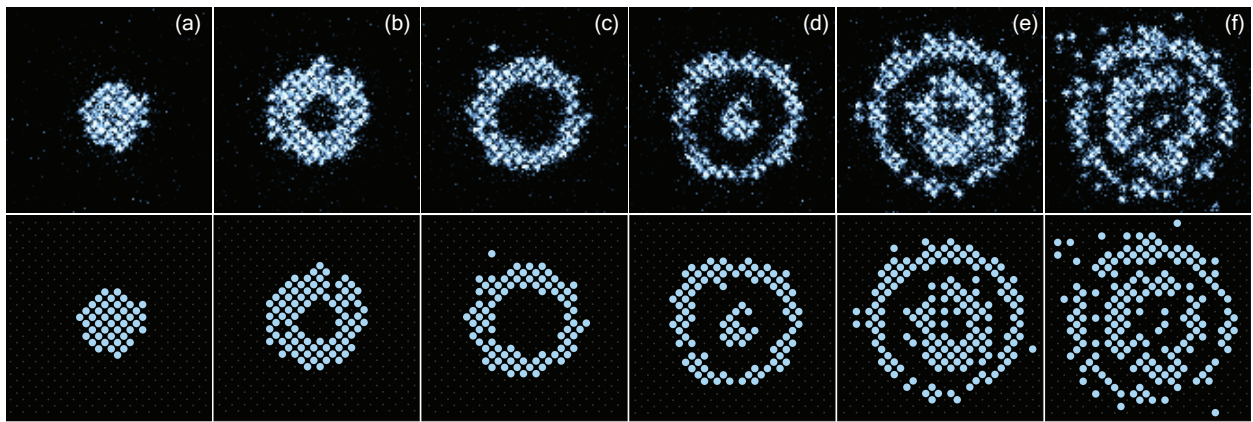


FIG. 2. Site-resolved imaging of a bosonic ^{174}Yb Mott insulator. Top row corresponds to raw images obtained with the emCCD camera during an exposure time of $40\ \mu\text{s}$. The bottom row shows the reconstructed atom density distribution obtained from the deconvolution algorithm. The estimated number of atoms in each image is (a) 45 ± 7 , (b) 115 ± 5 , (c) 179 ± 13 , (d) 273 ± 12 , (e) 486 ± 21 and (f) 592 ± 27 . Due to the presence of an external harmonic confinement in the optical lattices, the number of visible concentric Mott shells increases with the number of atoms.

compress the condensate utilizes the “optical accordion” technique described in [19, 20]. This technique consists in reflecting a laser beam from the flat substrate at a shallow angle to create a standing wave with manipulable periodicity. In contrast to the procedure explained in [19], which utilizes a combination of two orthogonal optical accordions and one vertical optical dipole trap (ODT), here we opt to perform evaporative cooling using only one accordion beam and the vertical ODT (see Fig. 1). Both beams have a wavelength of 1080.0 nm and propagate in the $x + y = 0$ vertical plane. After compressing the condensate, we perform a second evaporative cooling by reducing the accordion beam power in 9 s. We control the number of atoms loaded into the two-dimensional optical lattice by adjusting the final power of the accordion beam.

To load the atoms into the two-dimensional optical lattice, we use an additional pair of beams (wavelength 1080.0 nm) propagating in orthogonal planes $x = 0$ and $y = 0$. The lattice beams are reflected from the SIL at the same angle as the optical accordion and retro-reflected using a concave mirror with a 50 mm radius of curvature. This creates a two-dimensional lattice with spacing $a_{\text{lat}} = 543.5\text{ nm}$ in the $x - y$ plane and a standing wave with $4.8\ \mu\text{m}$ spacing in the z direction. The lattice beams have an elliptical waist of $26\ \mu\text{m}$ and $52\ \mu\text{m}$ in the z and $x(y)$ directions, respectively. We load the atoms in the lattice by ramping up the potential depth to $6.5 E_r$ in 2 s while decreasing the intensity of the vertical and accordion beams. At this point, atoms are in the superfluid regime, which we confirmed by the presence of sharp interference peaks in the momentum distribution[21]. We further increase the lattice depth using a smooth S-shaped curve to $26 E_r$ in 1 s to induce a phase transition to a Mott insulator[22].

We employ the photoassociation (PA) technique to remove pairs of atoms in multiply-occupied sites and realize parity measurement of the number density[23, 24]. The PA laser is red-detuned by 301 MHz from the $^1S_0 - ^3P_1$ atomic transition at 556 nm . Pairs of atoms decay in $34(22)\ \mu\text{s}$ for an optical lattice depth of $1200 E_r$ and a PA laser beam intensity of 0.75 W/cm^2 . For the experiment, we ramp up the lattice depth in 10 ms and irradiate the PA beam during 2 ms, which eliminates $> 99.9\%$ of the atom pairs and induces an average of ~ 0.5 photon scatterings in the rest of the atoms.

Finally, we obtain site-resolved imaging of a Mott insulator by further increasing the lattice depth to $3200 E_r$ in 5 ms and irradiating the excitation beam (wavelength 399 nm , intensity 65 W/cm^2) to the atoms for $40\ \mu\text{s}$. The scattered photons are collected by a high-resolution optical system (numerical aperture 0.81, magnification 110X) composed by the SIL and an objective lens and then focused into the emCCD camera (Andor iXon Ultra 888). The top row of Fig. 2 shows the obtained raw images for increasing number of atoms in the trap. The observed concentric shells correspond to a fixed number of atoms in each shell which is the characteristic structure of a Mott insulator in a harmonic confinement[25, 26]. To reconstruct the density distribution $n_{\text{det}}(\mathbf{r})$, we first estimate the total fluorescence in each site employing a computer algorithm based on deconvolution. The obtained total fluorescence is then compared with a previously determined fluorescence threshold to determine which site was occupied. The bottom row in Fig. 2 shows the estimated density distribution corresponding to each of the images on the top.

Next, we study the fidelity of our imaging system. In site-resolved imaging devices which rely on a cooling-based scheme to pin the atoms during the imaging pro-

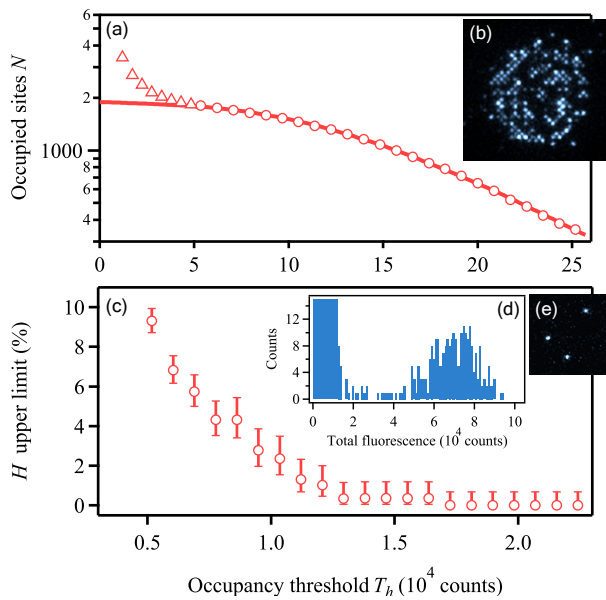


FIG. 3. Fidelity analysis for the noncooled approach. (a) The fraction of lost atoms is computed by analyzing the number of occupied sites as a function of the occupancy threshold in CCD counts for 100 images taken at an exposure time of $300\mu\text{s}$. The experimental data (circular points) is fitted using a Monte Carlo simulation (solid line), from which the survival rate function of atoms is obtained. Triangular points correspond to background events and are not included in the fitting. The estimated fraction of lost atoms is $L = 1.8\%$ for $T_h = 20000$ counts. (b) Raw image using an exposure of $300\mu\text{s}$. (c) Hopping probability H is obtained using 100 images with a sparse population containing an average of 2.6 atoms per image taken at an exposure time of $40\mu\text{s}$, from where the number of pairs of neighboring occupied sites is calculated. This value establishes an upper limit for the hopping. Error bars denotes 68% Clopper-Pearson confidence intervals. Hopping probability for $T_h = 20000$ counts is $H < 0.7\%$. (d) Histogram of the total site fluorescence for the sparsely occupied images on (c). The left and right peaks correspond to empty and occupied sites, respectively. (e) Typically obtained image (raw) with sparse occupation used on (c) and (d).

cess, the conventional method to estimate hopping and loss effects is to take two successive fluorescence images and then compare the observed atomic density distribution. As atoms are thermally in equilibrium during laser-cooling, hopping and loss rates are constant. The comparison method provides, in consequence, a good estimation of both rates.

In the case of the noncooled approach, the temperature of atoms during imaging is not constant but continuously increasing. In consequence, the loss rate also increases on time resulting in a number trapped of atoms that do not decay exponentially. Here, to estimate the fraction of lost atoms, we take multiple images employing the same procedure as in Fig. 2, but using a longer exposure time ($300\mu\text{s}$ instead of $40\mu\text{s}$). Typically observed image is

shown in Fig. 3(b). When background events are negligible, the dependence of the number of occupied sites N on the occupancy threshold T_h is given by the survival probability function $S(T_h)$ multiplied by the initial number of occupied sites N_0 . For small T_h , the background events become large. We identify these points and remove them from the analysis (triangular points in Fig. 3(a)). If $S(T_h)$ is known for every T_h , the fraction of lost atoms L can be estimated as $L = 1 - S$.

We fit the experimental data (circular points in Fig. 3(a)) using the $S(T_h)$ function obtained from a Monte Carlo simulation accounting losses due to heating and light-induced excitations from the optical lattice[19]. From the fitting, we determine the initial number of occupied sites ($N_0 = 1895$) and the fraction of lost atoms $L = 1.8\%$ for a threshold set at $T_h = 20000$ counts. Note that background events are sufficiently small for this threshold when the exposure time is $40\mu\text{s}$ (see Fig. 3(d)).

For the hopping probability H estimation we obtain 100 images (exposure time $40\mu\text{s}$) of lattices with sparse population containing an average of 2.6 atoms (see Fig. 3(e)). These samples are prepared by ramping down the lattice depth to $4E_r$ in 1 ms followed by a 0.5 s hold time. The shallow lattice depth allows atoms to disperse randomly along the lattice while the total number of atoms is reduced. The lattice depth is then ramped up to $26E_r$ in 10 ms to freeze the position of the atoms, and later imaged in the same way as the Mott insulator. For a given T_h , we calculate the probability of observing two occupied neighboring sites (see Fig. 3(c)). If the images contain only a few atoms and are sparsely populated, the probability of having two atoms occupying adjacent sites is very small. The plot in Fig. 3(c) gives, in consequence, a good estimation for H upper limit. We determine that $H < 0.7\%$ for $T_h = 20000$ counts, with a 68% confidence interval. The low hopping probability obtained here is a characteristic of the noncooled imaging system, as atoms that become heated are rapidly accelerated by the radiative force exerted by the excitation beam, and very rarely emit a sufficient number of photons in the neighboring sites to be considered occupied.

Finally, we perform temperature measurement of the atomic cloud by analysis of the reconstructed density distribution. The Bose-Hubbard model describes the behavior of atoms trapped in a two-dimensional optical lattice with harmonic confinement. When the tunneling rate J is sufficiently smaller than the on-site interaction energy U ($U/J \gg 16.7$)[27], the number density after parity projection $n_{\text{det}}(\mathbf{r})$ is approximated to (zero-tunnelling approximation)[3]:

$$n_{\text{det}}(\mathbf{r}) = \frac{1}{Z} \sum_{n=1}^{\infty} \text{mod}_2(n) \exp \left[\frac{\mu(r)n - E_n}{k_B T} \right],$$

where Z is the grand canonical partition function, μ is

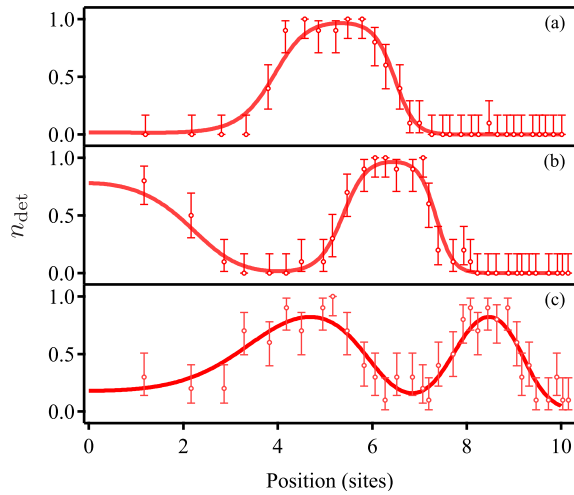


FIG. 4. Temperature measurement of a Mott insulator. Reconstructed atom density distribution is averaged azimuthally to obtain the radial profiles (points) and fitted using the grand-canonical ensemble described by the Bose-Hubbard model under the zero-tunneling approximation (solid lines). Error bars denotes 68% Clopper-Pearson confidence intervals. The experimental data for (a)-(c) correspond to the reconstructed density distributions (c), (d) and (f) in Fig. 2, respectively. From each fitting, the global chemical potential μ_0 , temperature T , and Mott radius r_0 are extracted.

the local chemical potential, T is the temperature, k_B is the Boltzmann constant and $E_n = Un(n-1)/2$ is the interaction energy for a site occupied by n atoms. We apply the local density approximation $\mu = \mu_0 - 0.5m\omega^2 r^2$ where μ_0 is the global chemical potential and ω is trap frequency of the harmonic confinement. Note that we consider an azimuthally symmetric function as we measured negligible ellipticity in our trap geometry.

We average the reconstructed number density azimuthally, and then fit the result with the theoretical $n_{\text{det}}(\mathbf{r})$ (see Fig. 4) taking the loss effects into account. From the fitting we extract the parameters μ_0/U , T/U and the Mott shell radius $r_0 = \sqrt{2U/m\omega^2}$. This yielded in the parameters $T = 0.10(1)U/k_B$, $\mu_0 = 1.56(6)U/k_B$, $r_0 = 5.1(1)a_{\text{lat}}$ for (a), $T = 0.10(1)U/k_B$, $\mu_0 = 2.14(4)U/k_B$, $r_0 = 5.0(1)a_{\text{lat}}$ for (b) and $T = 0.21(2)U/k_B$, $\mu_0 = 3.38(7)U/k_B$, $r_0 = 5.0(1)a_{\text{lat}}$ for (c). From the extracted parameters we also calculate the entropy per atom resulting in $0.32(6)k_B$ for (a), $0.28(4)k_B$ for (b) and $0.34(3)k_B$ for (c).

The errors in the computed parameter are caused by the limited number of sites used in the azimuthal average which is reflected by the size of the error bars in the experimental data. Hopping effects are very small and produce a negligible error in the measurement. Increasing the accuracy of this thermometer would require the use of traps having smaller ω or increasing U by using larger s-wave scattering lengths.

In conclusion, we have demonstrated the first site-resolved observation of a Mott insulator using a non-cooled method. This approach is robust against mechanical instabilities in the optical system owing to the short exposure time used during imaging. The simplicity of the setup using only one excitation beam that does not require retro-reflection makes it readily applicable to other species. In particular, lanthanoid atoms benefit from the noncooled method for having a large mass which results in small recoil energies ensuring small losses. We also show a method to estimate the loss and hopping effects and found that our system has comparable fidelity to that of the laser-cooling based counterparts. Our results are promising for the study of the Fermi-Hubbard model using a Yb gas in its generalized SU(N) form[28, 29]. Our preliminary results show observation of SU(6) Mott insulator of fermionic ^{173}Yb without any modification in the imaging setup, proving the flexibility of this system.

This work was supported by JSPS KAKENHI Grant Numbers JP17H02934, JP26800212, JP16F16029, and JP16K05498; the Tokyo Tech Suematsu Award, and the Research Foundation for Opto-Science and Technology. One of the authors (M.M.) is supported in part by the Japan Society for the Promotion of Science.

* miranda.m.aa@m.titech.ac.jp

- [1] W. S. Bakr, J. I. Gillen, A. Peng, S. Fölling, and M. Greiner, *Nature* **462**, 74 (2009).
- [2] W. S. Bakr, A. Peng, M. E. Tai, R. Ma, J. Simon, J. I. Gillen, S. Fölling, L. Pollet, and M. Greiner, *Science* **329**, 547 (2010).
- [3] J. F. Sherson, C. Weitenberg, M. Endres, M. Cheneau, I. Bloch, and S. Kuhr, *Nature* **467**, 68 (2010).
- [4] J. Simon, W. S. Bakr, R. Ma, M. E. Tai, P. M. Preiss, and M. Greiner, *Nature* **472**, 307 (2011).
- [5] P. M. Preiss, R. Ma, M. E. Tai, A. Lukin, M. Rispoli, P. Zupancic, Y. Lahini, R. Islam, and M. Greiner, *Science* **347**, 1229 (2015).
- [6] T. Fukuhara, P. Schausz, M. Endres, S. Hild, M. Cheneau, I. Bloch, and C. Gross, *Nature* **502**, 76 (2013), letter.
- [7] R. Islam, R. Ma, P. M. Preiss, M. Eric Tai, A. Lukin, M. Rispoli, and M. Greiner, *Nature* **528**, 77 (2015), article.
- [8] M. F. Parsons, F. Huber, A. Mazurenko, C. S. Chiu, W. Setiawan, K. Wooley-Brown, S. Blatt, and M. Greiner, *Phys. Rev. Lett.* **114**, 213002 (2015).
- [9] A. Omran, M. Boll, T. A. Hilker, K. Kleinlein, G. Salomon, I. Bloch, and C. Gross, *Phys. Rev. Lett.* **115**, 263001 (2015).
- [10] L. W. Cheuk, M. A. Nichols, M. Okan, T. Gersdorf, V. V. Ramasesh, W. S. Bakr, T. Lompe, and M. W. Zwierlein, *Phys. Rev. Lett.* **114**, 193001 (2015).
- [11] E. Haller, J. Hudson, A. Kelly, D. A. Cotta, B. Peaudecerf, G. D. Bruce, and S. Kuhr, *Nat Phys* **11**, 738 (2015), letter.
- [12] G. J. A. Edge, R. Anderson, D. Jervis, D. C. McKay,

- R. Day, S. Trotzky, and J. H. Thywissen, *Phys. Rev. A* **92**, 063406 (2015).
- [13] D. Greif, M. F. Parsons, A. Mazurenko, C. S. Chiu, S. Blatt, F. Huber, G. Ji, and M. Greiner, *Science* **351**, 953 (2016).
 - [14] L. W. Cheuk, M. A. Nichols, K. R. Lawrence, M. Okan, H. Zhang, and M. W. Zwierlein, *Phys. Rev. Lett.* **116**, 235301 (2016).
 - [15] A. Mazurenko, C. S. Chiu, G. Ji, M. F. Parsons, M. Kanász-Nagy, R. Schmidt, F. Grusdt, E. Demler, D. Greif, and M. Greiner, *arXiv preprint arXiv:1612.08436* (2016).
 - [16] D. Rossini and R. Fazio, *New Journal of Physics* **14**, 065012 (2012).
 - [17] S. Baier, M. J. Mark, D. Petter, K. Aikawa, L. Chomaz, Z. Cai, M. Baranov, P. Zoller, and F. Ferlaino, *Science* **352**, 201 (2016).
 - [18] R. Yamamoto, J. Kobayashi, T. Kuno, K. Kato, and Y. Takahashi, *New Journal of Physics* **18**, 023016 (2016).
 - [19] M. Miranda, R. Inoue, Y. Okuyama, A. Nakamoto, and M. Kozuma, *Phys. Rev. A* **91**, 063414 (2015).
 - [20] M. Miranda, A. Nakamoto, Y. Okuyama, A. Noguchi, M. Ueda, and M. Kozuma, *Phys. Rev. A* **86**, 063615 (2012).
 - [21] M. Greiner, O. Mandel, T. Esslinger, T. W. Hansch, and I. Bloch, *Nature* **415**, 39 (2002).
 - [22] The superfluid-to-Mott-insulator transition is expected to occur at a lattice depth of $15 E_r$. At $26 E_r$ the tunneling rate becomes negligible compared with the on-site interaction and fluctuations in the atom number are drastically reduced.
 - [23] S. Tojo, M. Kitagawa, K. Enomoto, Y. Kato, Y. Takasu, M. Kumakura, and Y. Takahashi, *Phys. Rev. Lett.* **96**, 153201 (2006).
 - [24] S. Sugawa, K. Inaba, S. Taie, R. Yamazaki, M. Yamashita, and Y. Takahashi, *Nat Phys* **7**, 642 (2011).
 - [25] B. DeMarco, C. Lannert, S. Vishveshwara, and T.-C. Wei, *Phys. Rev. A* **71**, 063601 (2005).
 - [26] S. Fölling, A. Widera, T. Müller, F. Gerbier, and I. Bloch, *Phys. Rev. Lett.* **97**, 060403 (2006).
 - [27] S. Wessel, F. Alet, M. Troyer, and G. G. Batrouni, *Phys. Rev. A* **70**, 053615 (2004).
 - [28] C. Hofrichter, L. Riegger, F. Scazza, M. Höfer, D. R. Fernandes, I. Bloch, and S. Fölling, *Phys. Rev. X* **6**, 021030 (2016).
 - [29] C. Honerkamp and W. Hofstetter, *Phys. Rev. Lett.* **92**, 170403 (2004).